Original Article

Diffusion of neutral solutes within human osteoarthritic cartilage: Effect of loading patterns

Haoye Meng [a,b,c,☆], Qi Quan [b,☆], Xueling Yuan [b], Yudong Zheng [a,*], Jiang Peng [b,c], Quanyi Guo [b,c], Aiyuan Wang [b,c,**], Shibi Lu [b,c]

[a] School of Material Science and Engineering, University of Science and Technology Beijing, Beijing, China
[b] Institute of Orthopaedics, Chinese PLA General Hospital, Beijing, China
[c] Beijing Key Lab of Regenerative Medicine in Orthopaedics, Beijing, China

ABSTRACT

Objective: Variation of the solute diffusion within articular cartilage is an important feature of osteoarthritis (OA) progression. For *in vitro* study of monitoring of the diffusion process, it is essential to simulate physiological conditions as much as possible. Our objective was to investigate the effects of loading patterns on diffusion processes of neutral solutes within osteoarthritic cartilage.

Methods: Osteochondral plugs were harvested from human tibial plateaus and separated into three OA stages according to modified Mankin scoring system. The samples were subjected to static or cyclic compression using a carefully designed loading device. Contrast-enhanced micro-computed tomography (CEμCT) was applied to acquire image sequences while the cartilage was being compressed. The apparent diffusion maps and diffusion coefficients were analysed, as well as histological and stereological assessments of the plugs.

Results: The diffusion of neutral solutes was significantly affected by the loading patterns. For OA cartilage with early and middle stages, cyclic loading accelerated contrast agent infiltration compared with static loading. However, for late-stage OA samples, no acceleration of diffusion was observed in the first 2 h because of the insufficient resilience of compressed cartilage. The accumulation of neutral solutes in an upward invasive fissure also suggested that solutes could penetrate into the fissure under cyclic loading.

Conclusions: To our knowledge, this is the first study to combine the cyclic compression and CEμCT scanning in the diffusion testing of human OA cartilage. This loading pattern could simulate the physiological conditions and reduce the time to reach solute equilibrium within cartilage. The diffusion data may contribute to joint drug-injection therapies for early OA.

The translational potential of this article: The combination of cyclic loading and CEμCT scanning enabled diffusion analysis of osteoarthritic cartilage under different compressions. A comprehensive evaluation of OA cartilage and subchondral bone may benefit from this technique. The diffusion data provide theoretical support and reference for intra-articular injection of drugs.

Introduction

In healthy joints, articular cartilage is a highly organised avascular tissue. The cartilage matrix consists of 10–30% collagen and 3–10% proteoglycans (PGs), with water and dissolved electrolytes filling the intervening spaces and accounting for 60–85% of the tissue's total weight. These primary components form an intricate network that allows cartilage to resist compressive loads and determines whether molecules can penetrate the matrix [1]. Cartilage metabolism depends on molecular diffusion from synovial fluid and subchondral bone. Common nutrients and regulatory substances must travel through the compact matrix to reach the chondrocytes. Therefore, the permeability of cartilage, which describes the ease of molecules penetrating, has attracted a lot of research interest. Several recent studies have confirmed that molecular

Figure 1. (A) Schematic of specimen preparation. Local enlarged area indicates the diseased cartilage under physiological load (a1). Osteochondral plugs (φ = 16.3 mm) were extracted from the loading regions of medial and lateral plateaus in the OA joint (a2). **(B)** Plugs were mounted in the custom-made loading device (b1). Contrast agent could only enter the cartilage through the micro-channels in the porous piston indenter. The µCT image showed that X-ray absorption of this device was similar to that of cartilage (b2). **(C)** Time points of µCT imaging in event sequence. Two types of loading were applied to osteochondral plugs: static and cyclic compression. Self-diffusion was used for comparison. **(D)** Evaluation subjects of samples: µCT imaging (d1), apparent color mapping and diffusion analysis (d2), Safranin-O/Fast Green staining (d3, bar = 200 µm), and stereology assessment of the subchondral bone (d4).

Table 1
Detailed information of the samples.

OA stage	Amount of tibial plateau	Treatments	Amount of osteochondral plugs	Cartilage thickness (mm)	Modified Mankin grading[b]			Type of diffusion		
					Structure (0–6)	Cellular abnormalities (0–3)	Matrix staining (0–4)	Self-diffusion	Static compression diffusion	Cyclic compression diffusion
Early	4	TKA[a] (2), Amputees (2)	n = 8	2.53 ± 0.27	0.75 ± 0.71	0.63 ± 0.51	0.75 ± 0.46	n = 2	n = 3	n = 3
Middle	7	TKA	n = 12	1.87 ± 0.38	3.12 ± 0.72	1.42 ± 0.90	1.92 ± 0.67	n = 3	n = 3	n = 6
Late	10	TKA	n = 12	1.43 ± 0.54	4.92 ± 0.51	2.08 ± 0.51	3.50 ± 0.67	n = 3	n = 4	n = 5

[a] TKA: total knee arthroplasty, data are shown as mean ± SD.
[b] The modified Mankin score was calculated as a mean of three evaluations independently conducted by three investigators from blind-coded samples.

crosstalk occurs between cartilage and subchondral bone [2,3]. In addition, a "pumping effect," generated by cartilage compression under physiological loading, may be responsible for transporting substances within cartilage [4]. Matrix stabilisation, structural integrity, and type of loading are among the many factors that can affect the permeability.

Osteoarthritis (OA) is a severe joint disease characterised by pathological processes in both cartilage and subchondral bone [2,5]. The signs include depletion of PGs, deterioration of the collagen network, and remodelling of the subchondral bone. These complex changes inevitably affect molecular diffusion between adjacent layers of cartilage. Deep fissures or fractures within the osteochondral interface have been proved to participate in molecular exchange and transport of substances [6]. Because joints are generally subjected to physiological compression and cyclic loading, biomechanical factors also need to be considered in analysing the diffusion process of cartilage [7,8]. As mentioned above, static and cyclic loading on cartilage can lead to a "pumping effect." If the type of loading is altered, as in OA joints, the cartilage and subchondral bone undergo structural changes, which may affect their permeability [9]. Felson et al., from a biomechanical point of view, described how mechanically induced injury to joint tissues is a contributory factor in nearly every case of OA [5]. A previous study by Shafieyan et al. explored aspects of solute transport within cartilage relevant to static compression [10]. Quinn et al. also reported that static compression of articular cartilage can reduce solute diffusion and partitioning within the matrix [11]. Recent studies have investigated more realistic simulations of

solute transport in animal and human cartilage undergoing cyclic deformation [12,13].

However, efforts to understand diffusion have mainly focused on theoretical simulation, mathematical modelling, and quantification of cartilage compositions [7,14]. Although these information would be valuable for detecting physiological changes in cartilage at an early stage of OA, current data on permeability in response to different mechanical factors do not explicitly support an optimal type of loading for assessing the permeability of OA cartilage.

We therefore aimed to directly visualise the diffusion process of neutral solutes in OA cartilage subjected to cyclic compressions using the contrast agent-enhanced computed tomography (CECT) technique and investigate the effects of loading patterns on the permeability of cartilage at different stages of OA. We applied cyclic deformations to cartilage *in vitro* using a custom-made device and simultaneously examined solute diffusion within the cartilage. The free and statically compressed diffusions were also performed for comparison. Other factors, including loss of cartilage composition and structural changes in subchondral bone, were investigated by pathological and stereological analyses.

Materials and methods

Specimen preparation

The study design was descriptive. Human tibial plateaus (n = 19, 12
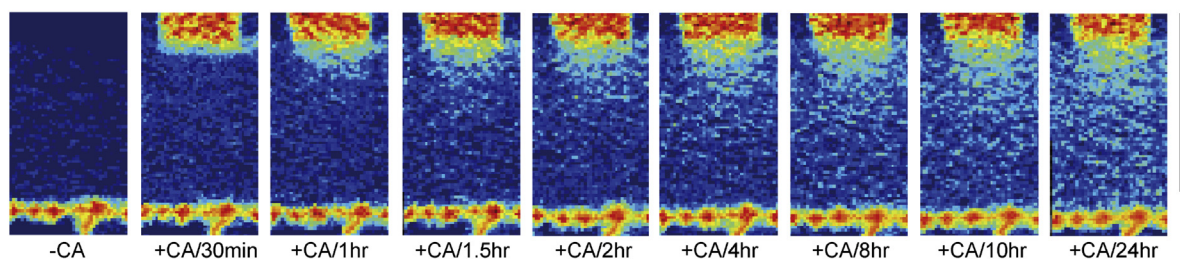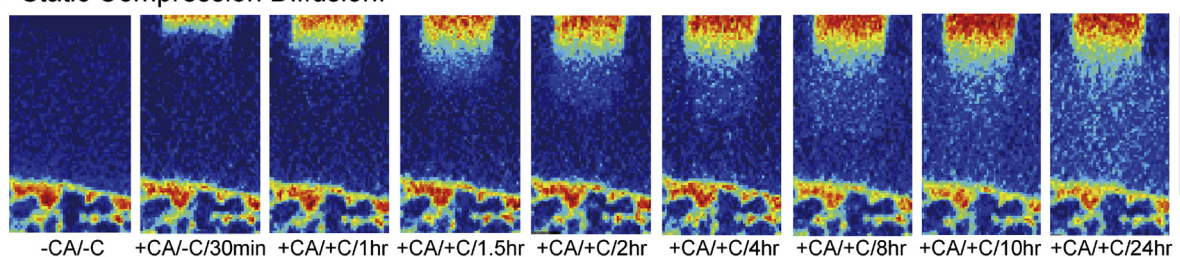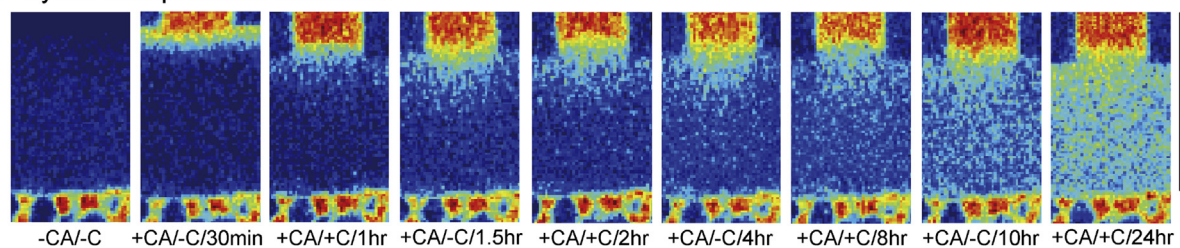
Figure 2. Typical apparent diffusion mapping of contrast agent within the early-stage OA cartilage. Static compression diffusion group showed the slowest infiltration rate throughout the test period (**A**). The self-diffusion group and cyclic compression diffusion group got similar results over the first 1.5 h. In the latter part of test period, the penetration of contrast agent was faster in samples from the cyclic compression diffusion group (**B**) than in those from the self-diffusion group (**C**). At 24 h, only cartilage from the cyclic compression diffusion group was 50% saturated. The images at each time point are not fully displayed. Minor scale = 500 μm.

females and 7 males) were harvested from OA patients with a level of evidence II (age range: 46–71 years) who were undergoing total knee arthroplasty (*operation period: November 2016–May 2017, agreed and signed informed consent*). Two more plateaus (of a 47-year-old male and a 52-year-old female) were obtained with consent from amputees without tumor invasion or knee fracture (*crush injuries in the lower extremities, operation time: June 2016 and October 2016*). Approval for this work was obtained from the Institutional Review Board of the People's Liberation Army General Hospital, Beijing, China. Within 2 h of obtaining the plateaus, osteochondral plugs (n = 32, 19 females and 13 males) were extracted using a 16.3 mm diameter trephine from the loading regions of the medial and lateral plateaus (Figure 1 A). To avoid denaturing the cartilage proteins, the plugs were kept moist with phosphate buffered saline (PBS) containing metalloproteinase inhibitors. The annular outer edge of each plug and the adjacent osteochondral fragment from each plateau were prepared for histological analyses. The samples were graded by visual inspection and histopathology assessments according to the modified Mankin scoring grading [15,16]. To maintain consistent thickness and fit into the device, the bone part was incised to a uniform thickness of 4 mm, and the thickness of subchondral bone plate ranged from 1.3 mm to 2.7 mm according to the stage of OA. Detailed information about the samples in each group is shown in Table 1.

Loading protocols and CECT image acquisition

The custom-made cyclic compression holder was made of acrylic, which does not strongly attenuate X-rays and has high stiffness compared to cartilage. The holder had two chambers connected by a concentric circular channel (Φ = 10 mm) (Figure 1B). A porous acrylic piston was fitted tightly within the channel and functioned as an indenter. The upper platen had a calibrated scale and could be screwed into the chamber to contact the top of the piston. When rotated clockwise one full scale, the piston moved downward approximately 0.5 mm (0.1 mm/grid). The cylindrical plug was fixed at the top of the lower chamber with the radial edges of cartilage against the boundary of the channel, exposing a circular region of cartilage surface to the base of the piston. The contrast agent could only enter the cartilage through the micro-channels (Φ = 0.8 mm) in the porous piston. Another platen could be screwed into the lower chamber to support the osteochondral plug. For early OA stage, the piston moved downward 0.3 mm–0.5 mm at 0.1 mm/s. For middle and late OA stage, the displacement of piston was 0.1 mm–0.3 mm at 0.1 mm/s. Less than 15% strain would not result in significant cartilage damage [14,17].

Iohexol ($C_{19}H_{26}I_3N_3O_9$, M = 821.14 g/mol, Omnipaque®, GE healthcare, Chicago, IL, USA) was chosen as the non-ionic contrast agent.
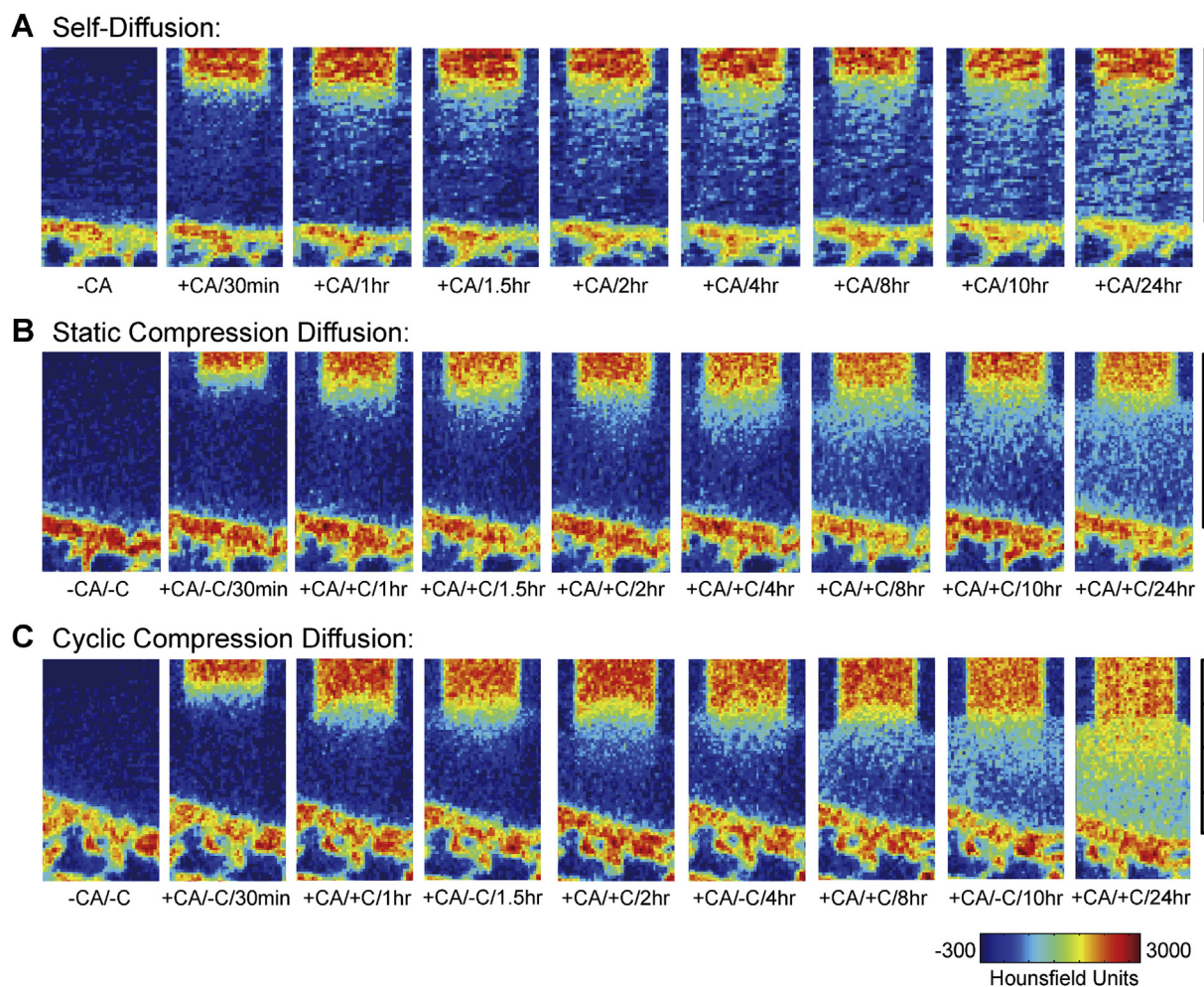
Figure 3. Typical apparent diffusion mapping of contrast agent within the middle stage-OA cartilage. The static compression diffusion group showed the slowest infiltration rate throughout the test period the the self-diffusion group (A) was more than that in the cyclic compression diffusion group (B). In the first 4 h, the concentration of contrast agent in the self-diffusion group (C). In the latter part of the test, cartilage from the cyclic compression diffusion group was 76% saturated and significantly different with the other two groups. The images at each time point are not fully displayed. Minor scale = 500 μm.

It is commonly used in clinical computed tomography (CT) examinations. The osmolality of the solution was 410 mOsm/L and the pH was 7.4, which is similar to the *in situ* osmolality of articular cartilage (350–450 mOsm/kg). The contrast agent solution was mixed by gentle agitation before it was injected into the upper chamber (Figure 1B). The tests were performed at ambient temperature (25 ± 1 °C).

The samples were categorised into two groups according to the types of loading applied: static compression diffusion group (SCD, n = 10) and cyclic compression diffusion group (CCD, n = 14). A self-diffusion group (SD, n = 8) was used for comparison. The sequence of events is shown in Figure 1C. For static compression diffusion, 5 mL iohexol solution was injected into the chamber and allowed to contact with the surface of the cartilage. Then the upper platen was rotated 6° clockwise and confined compression was maintained until the end of the test. Images were acquired at each pre-defined time point as shown in Figure 1C. For cyclic compression, the indenter was unloaded at each time interval using counterclockwise rotation (under otherwise identical conditions). The loading cycles were repeated in sequence and followed by CT imaging at each time point. For the self-diffusion group, the porous piston gently contacted the cartilage surface and the iohexol solution naturally diffused into the cartilage. All images were acquired using a micro-CT instrument (GE healthcare, USA). The total imaging time was approximately 17 min. The X-ray settings were standardised to 84 kVp and 175 μA with an exposure time of 0.3 s/frame. The CT slice was 45 μm thick and the in-plane pixel size was 45 × 45 μm^2.

Diffusion analyses

The CECT imaging analysis protocol was similar to the method described by Silvast et al. [18–20]. The X-ray absorption maps were first transformed linearly to generate contrast agent distribution maps [21]. Our method used a different reference parameter for conversion. Based on micro-CT analysis software (Micro View™ ver.2.2), contrast agent concentrations were quantified by bone mineral content (BMC, mg). The contrast agent concentration inside the cartilage was defined as moles of solute per volume of tissue. The BMC values represented the mineral concentration within three-dimensional structures instead of apparent two-dimensional sections. This conversion was also used to simplify subsequent calculations of the diffusion flux and the diffusion coefficient of contrast agent. The conversion equations were obtained from polynomial fitting of a calibrated series of known iohexol dilutions, as follows:

$$C = 0.078 \times BMC^2 + 0.035 \times BMC + 0.004 \qquad R^2 = 0.994, \qquad (1)$$

where C is the concentration of iohexol (mMol) and BMC is the bone mineral content of selected region (mg).

Gray-scale histogram analyses were performed to find an optimal threshold (800 Hounsfield unit) for the BMC calculation and to subtract the initial BMC of native cartilage and subchondral bone [22]. We assumed that cartilage was radially homogeneous and that diffusion was
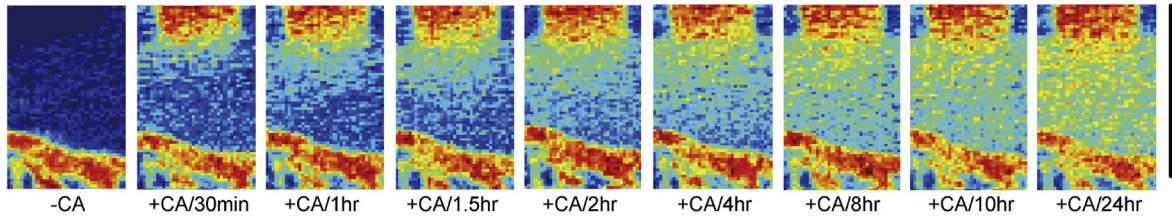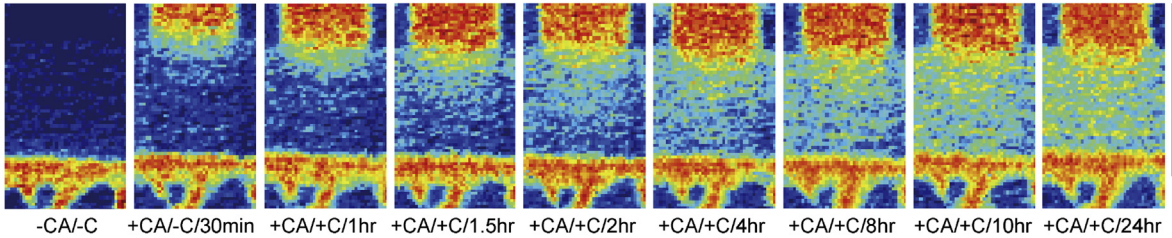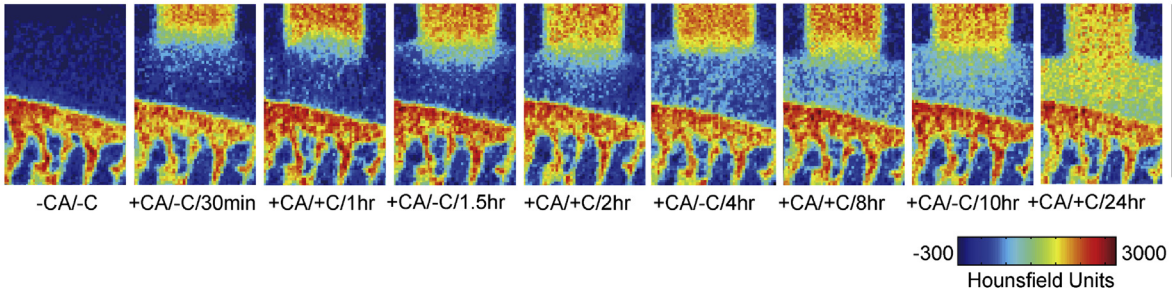
Figure 4. Typical apparent diffusion mapping of contrast agent within the late stage OA cartilage. (A) Diffusion process of self-diffusion group, (B) Diffusion process of static compression diffusion group, (C) Diffusion process of cyclic compression diffusion group. The intensity of contrast agent increased strongly in each group, and from the 8 h time point onwards, the contrast agent nearly reached equilibrium. The concentration of contrast agent within cartilage did not significantly increase when loading was removed in cyclic compression diffusion group. This was particularly evident in 1-1.5 h and different with same group samples in the early and middle stages of OA. The images at each time point are not fully displayed. Minor scale=500μm.

restricted only from superficial cartilage into the deep layer, which is non-convective and non-reactive. According to Fick's laws, the diffusion coefficient (D) and flux (J, moles of contrast agent per s per μm^2 of transverse section) can be expressed as:

$$J = -D\frac{\partial C}{\partial x} \tag{2}$$

where $\frac{\partial C}{\partial x}$ is the concentration gradient of iohexol across the depth of the cartilage. Combining Eq. (2) with iohexol solute continuity gives:

$$\frac{\partial C}{\partial t} = D\frac{\partial^2 C}{\partial x^2} \tag{3}$$

where t is the time. For the boundary condition, the concentration of contrast agent at the diffusion interface was assumed to be constant. A total of nine volumes of interest (VOI) from each sample were manually demarcated in cartilage under the porous piston and the mean value was calculated. The width was set to 30 pixels, which was greater than the diameter of the channels in the piston. The height of the VOI was adjusted to the full thickness of the cartilage. The total number of the VOI for cartilage diffusion analysis was 288. To visualise contrast agent distribution at different time points across the depth of the cartilage [23, 24], the same cross-section of CT images was rendered to a color map using custom-made MATLAB scripts (R2008a, MathWorks Inc., Natick, MA, USA).

Histological and stereological assessments

After CECT imaging, samples and adjacent fragments were assessed histologically. Following fixation in 4% paraformaldehyde in PBS (pH 7.4, 4 °C), the osteochondral plugs were decalcified in 15% EDTA (pH 8.5, 37 °C) for 3 weeks, embedded in paraffin, and sectioned at 200 μm intervals into a series of 5 μm thick sections. The slides were stained with Safranin-O/Fast Green to assess the damage to the cartilage (modified Safranin-O/Fast Green FCF Cartilage Stain Kit, Solarbio Life Sciences, Beijing, China). To match the histological staining image with the CT image at the same position, additional marks were made on the plugs.

The CECT method also facilitated stereological assessments of the subchondral bone plate. Three-dimensional CT image datasets were visualised after refined reconstruction. At the center of the subchondral bone plate, a cylindrical region of interest (Φ = 90, h = 30 pixels) was selected for stereological analyses. The mean thickness of the subchondral bone plate and the trabecular network stereology was calculated using Advanced Bone Analysis (ver. 2.0, Micro View™).

Statistical analysis

All data are reported as mean ± standard deviation. Statistical analyses were performed using statistical product and service solutions (SPSS, ver. 22.0; SPSS, Inc., Chicago, IL, USA). To assess the diffusion coefficients of iohexol and stereological parameters of the subchondral
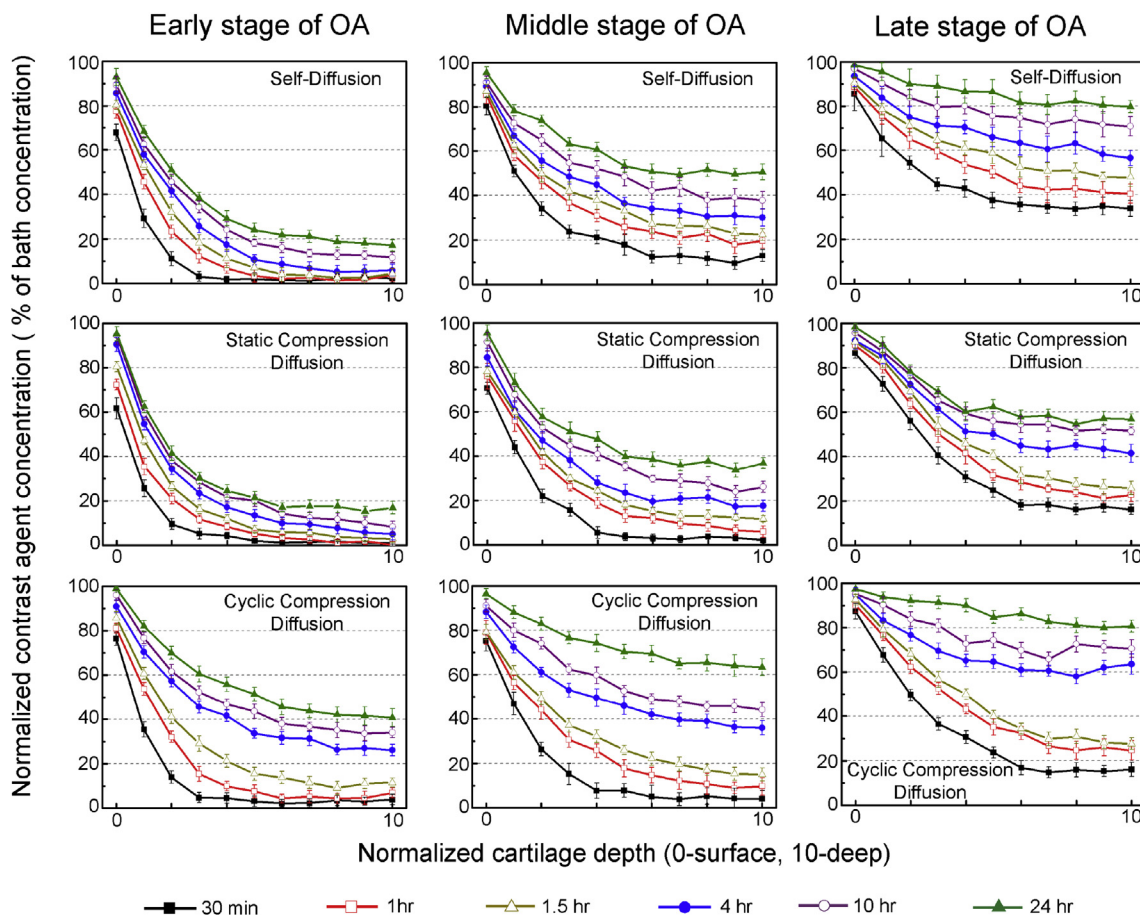
Figure 5. Diffusion curves of normalised contrast agent concentration–cartilage depth. In each group, equilibrium concentrations of contrast agent at 24 h were lower under static compression than under other loading patterns. Cyclic loading accelerated contrast agent infiltration within the cartilage in different stages of OA, reducing the time taken to reach a particular concentration at the same depth in cartilage. In late-stage OA samples, the 1 h/with compression diffusion curve gets close to the 1.5 h/without compression diffusion curve. The curves at each time point are not fully displayed. Data are shown as mean ± SD, n = 10 for each group.

bone, one-way analysis of variance (ANOVA) was used to compare differences between three groups, and *p < 0.05 was considered statistically significant.

Results

Apparent diffusion mapping and curves

The colored diffusion maps showed differences in X-ray absorption in each of the samples (Figures 2–4). The infiltration of contrast agent into the cartilage was significantly different among the three test procedures.

For the early stage of OA, the SCD group showed the slowest infiltration rate throughout the test period (Figure 2B). Although the SD and CCD groups showed similar results over the first 1.5 h, the penetration of iohexol in the CCD group was faster than in the SD group after 8 h (Figure 2A and C). At 24 h, only the CCD group was 50% saturated (Figure 2C). Similar results were observed for samples in the middle stage of OA (Figure 3). For samples in a late stage of OA, the intensity of iohexol increased strongly in each group (Figure 4). From the 8 h time point onwards, the SD and SCD group samples were almost saturated with iohexol and had nearly reached equilibrium.

However, when loading was removed, the iohexol content in the cartilage from the CCD group did not significantly increase. This was particularly evident in 1–1.5 h and different with CCD group samples in the early and middle stages of OA.

The apparent diffusion curves are shown in Figure 5. In each group, equilibrium iohexol concentrations at 24 h were lower under static

Table 2
Diffusion coefficient (mean ± SD) for different layers within the cartilage. The cartilage sections were divided into three equal layers along the thickness.

OA stage	Loading patterns	Average diffusion coefficient (μm²/s)		
		Through the superficial layer	Through the intermediate layer	Through the deep layer
Early	SD	37.89 ± 5.22	26.23 ± 5.08	17.48 ± 4.36
	SCD	21.86 ± 4.86	14.57 ± 4.23	8.74 ± 2.39
	CCD	39.43 ± 5.53	27.45 ± 4.94	23.17 ± 3.97
Middle	SD	52.01 ± 8.87	43.28 ± 7.49	26.94 ± 5.32
	SCD	31.44 ± 6.74	13.03 ± 4.04	9.77 ± 2.43
	CCD	47.15 ± 8.09*	49.03 ± 7.43*	33.95 ± 6.53*
Late	SD	81.43 ± 11.12	61.72 ± 9.45	48.64 ± 8.73
	SCD	69.95 ± 10.27	53.49 ± 8.14	27.78 ± 4.96
	CCD	89.51 ± 12.93*	70.98 ± 11.41*	41.67 ± 7.15

For middle and late stages of OA, the diffusion coefficient through superficial and intermediate layers of the CCD group was significantly higher than that of the SCD and SD groups. Data are shown as mean ± SD, *p < 0.05, Wilcoxon signed-ranks test, n = 10 for each group; SD: self-diffusion, SCD: static compression diffusion, CCD: cyclic compression diffusion.

compression than under other loading patterns. Cyclic loading accelerated iohexol infiltration in all stages of OA. However, in late-stage OA samples, the 1 h/with compression and 1.5 h/without compression diffusion curves were similar. This indicates that the concentration of iohexol did not increase immediately after compression was removed.
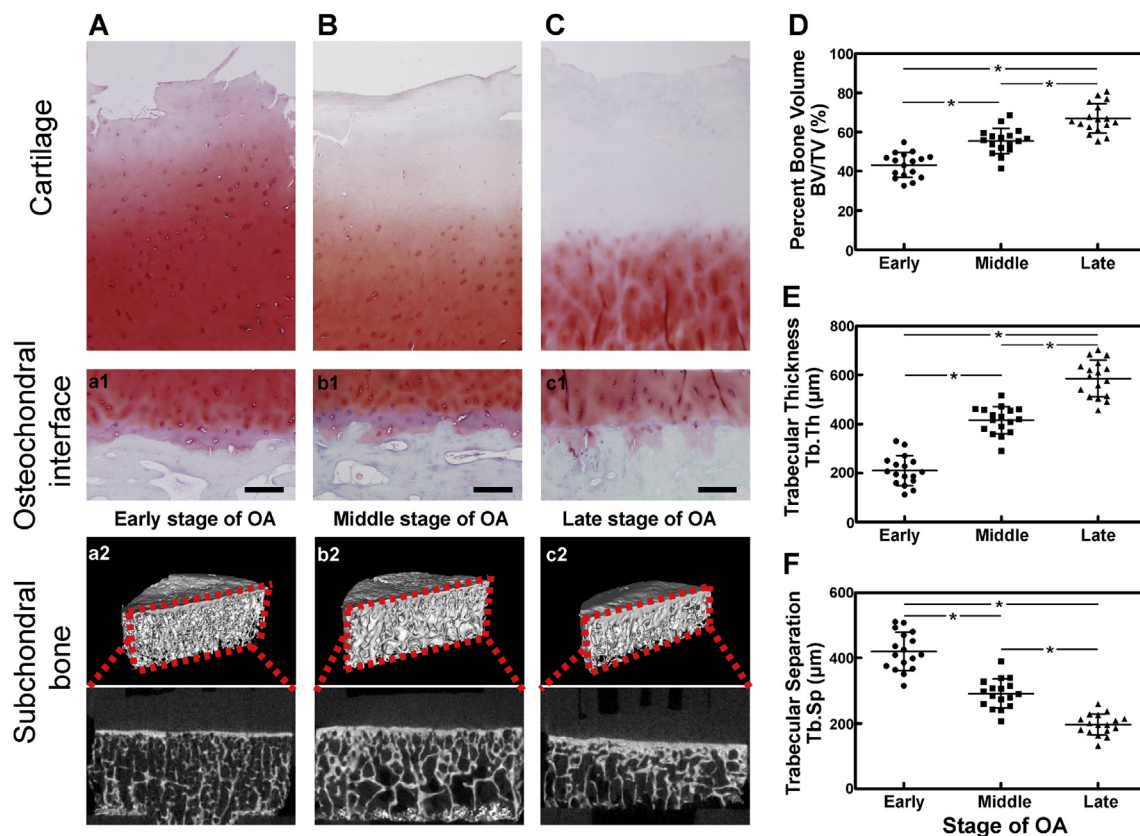
Figure 6. Representative Safranin-O/Fast Green staining of osteochondral plugs and stereological analyses of the subchondral bone. (A) A slight reduction of PGs present in the superficial layer of cartilage. Osteochondral interface remains continuous and intact (a1). **(B)** A moderate reduction of PGs is exhibited in the layer of cartilage. Tidemark was irregular and breached by fissures and the subchondral bone (b1). **(C)** A severe loss of PGs within the upper third of the cartilage. The thickness of the subchondral bone increased with decreasing of pores and cracks in the osteochondral interface. (a2–c2) Three-dimensional structure and μCT image of the subchondral bone in early, middle, and late stages of OA. **(D, E)** Percent of bone volume and trabecular thickness of subchondral bone significantly increased with OA progression. Trabecular separations significantly decreased with OA progression **(F)**. Data are shown as mean ± SD, n = 17, *P < 0.05 for between-group comparisons. Scale bars represent 200 μm.

Diffusion coefficients with cartilage depth

The mean diffusion coefficients for contrast agent in different cartilage layers are shown in Table 2. Deeper cartilage generally had lower diffusion coefficients. In the SD group, the reductions were 45%, 30%, and 16% for early-, middle-, and late-stage samples, respectively. The diffusion coefficients observed in response to different loading patterns showed similar trends. The coefficient for the SCD group was significantly lower than that for the CCD group (p < 0.05, n = 10).

Histological observations

The pathological staining results were consistent with typical features of OA. Safranin-O/Fast Green staining showed different degrees of PG depletion (Figure 6A–C). During the early stages of OA, a slight reduction in PGs is present in the superficial layer of cartilage. The chondrocytes were distributed throughout the cartilage layers. However, in samples with late stage of OA, there was a clear reduction in the level of Safranin-O staining within the upper third of the cartilage. The number of chondrocytes in the deeper layers was also reduced. In the middle/late stage of OA, the tidemark was irregular and breached by fissures and subchondral bone. In addition, the thickness of the subchondral bone increased gradually and the number of pores and cracks decreased, particularly during the late stages of OA. Overall, the histological evaluation showed clear variation in the PG content and structural deterioration at the osteochondral interface.

Stereological assessments

Stereological analyses of the subchondral bone revealed an OA stage-dependent trend. The thickness of the subchondral bone plate increased as the bone volume/total volume increased from 42% to 68%. The bone micro-morphometric parameter results indicate that the separations of trabecular bone became significantly smaller, whereas the bone itself became gradually thicker as OA processed (Figure 6D–F). More interestingly, we identified a fissure in the osteochondral interface from the apparent diffusion CT images. Safranin-O/Fast Green staining at this location showed that the fissure extended into the cartilage (Figure 7A). The concentrations of contrast agent at adjacent areas were calculated separately (Figure 7E). The results showed that the iohexol content in the selected deep cartilage zone (grid 4#, 5#, and 6#) had increased significantly during the test. In the subchondral bone zone, the content of contrast agent in grid 1# and 3# had not increased. The range was only from 0.05 ± 0.03 mM to 0.21 ± 0.08 mM. However, the content in the fissure (grid 2#) was accumulated from 0.07 ± 0.04 mM to 0.63 ± 0.12 mM. This indicated that contrast agent could penetrate into the fissure under cyclic loading.

Discussion

OA has been recognised as a process of simultaneous degradation of matrix and structure resulting from mechanically induced injury. In this study, we revealed the diffusion processes of a contrast agent within the
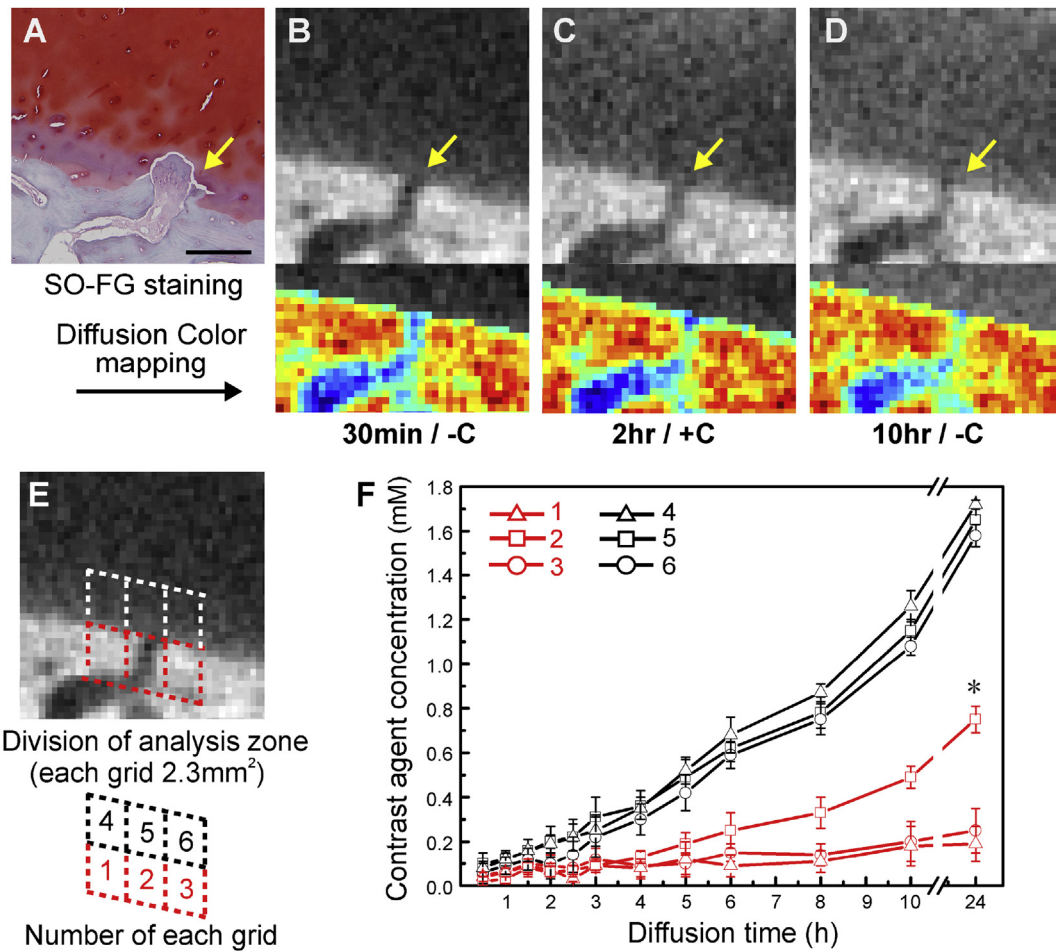
Figure 7. A fissure identified in the osteochondral interface from the apparent diffusion μCT images. (A) Safranin-O/Fast Green staining of fissure and adjacent tissue. (B-D) Apparent diffusion images and color mapping of osteochondral plugs under cyclic loading. (E) Two adjacent areas (white and red dash line) were analysed separately. (F) Contrast agent content in deep cartilage zone increased significantly (grid 4#, 5#, 6#, compared with 0h diffusion time). In the subchondral bone zone, the contrast agent in fissure (grid 2#) increased significantly compared with adjacent areas (grid 1#, 3#) at 24h, *P<0.05. Yellow arrow indicates the fissure in osteochondral interface, +/-C: with/without compression; Bar=200μm.

OA cartilage using CEμCT. In particular, we investigated the effects of loading patterns and OA grade on cartilage permeability. For the first time, cyclic compression followed by CEμCT scanning was applied on human OA osteochondral samples. Contrast agent diffusion was visualised using apparent color mapping. In addition, infiltration through micro-cracks in the subchondral bone was evaluated.

The loading pattern is one of the most important factor influencing diffusion. It was fully verified by apparent diffusion maps, curves, and coefficient results in this work. Compared to static loading, cyclic compression accelerated partitioning of the contrast agent within the cartilage layers. Early-stage OA samples in particular contained higher concentrations of contrast agent after unloading at each time point. This phenomenon has previously been described and suggests that, under cyclic loading, solutes are transported through the matrix by a 'pumping effect' [4]. However, for late-stage OA samples, cyclic compression did not significantly affect the diffusion process as expected. Although the contrast agent almost saturated the cartilage at 8 h, penetration of late-stage OA cartilage in the CCD group had not significantly increased after load had been removed at 1–1.5 h. This differed from the results obtained for the CCD group of early- and middle-stage OA samples. Research on the biomechanics of cartilage has shown that the elasticity decreases with OA progression [25]. The resilience of compressed cartilage from late-stage OA was inferior to that of early-stage samples. By combining the diffusion curve and cyclic deformation data, we infer that cartilage with insufficient resilience fails to absorb more contrast

agent than the fully restored cartilage. The permeability of SCD group samples in an early- or middle-stage of OA was lower than that of the SD group, despite a single and invariable compression being applied in this study. This is consistent with the study of Shafieyan et al. [10], who showed that static loading was associated with decreases in the diffusion of sodium iodide. Because the structure and compositions of early OA cartilage is relatively intact, reductions in permeability under static compression are reasonable. However, in late-stage OA cartilage, the severe structural disruptions lead to accelerated penetration of the contrast agent. The effects of compression on diffusion were not obvious, particularly the effects on later diffusion.

In addition, we found that deeper cartilage had a lower mean diffusion coefficient. This could be attributed to the more space, resulting from a decrease in the PG content and destruction of the collagen meshwork [26], within superficial layers for contrast agent. The loss of PGs within the matrix was evident along with the depth of OA cartilage. Although different contrast agents have been used, many studies have shown that changes in the composition and structure of cartilage can markedly affect fluid penetration [27]. Our color mapping images showed that the contrast agent had a tendency to accumulate in particular regions. These regions may be structurally weak or irregular, as described in the histologic assessments.

Stereological measurements of the subchondral bone plate were recorded to identify factors that might affect diffusion. However, in the literature, the effect of the subchondral bone on cartilage diffusion is still

controversial [28]. The low porosity of the subchondral bone was supposed to limit the fluid diffusion [6]. In another report by Hwang et al. [29], the hydraulic conductance of the subchondral bone plate increased as OA progressed. We focused on a fissure in the subchondral bone and identified the corresponding position in apparent diffusion images according to the histological observations. The accumulation of the contrast agent in this fissure space suggested that solute could penetrate through the fissure into the subchondral bone. Because of the μCT resolution and mismatches between the two types of image series, no more fissures were identified in the remaining samples. If exploring the relationship between this pathological change links with the contrast agent infiltration, more samples and precise matching techniques are required in the further work.

Some limitations in this study must be noted. As in other *in vitro* experiments, contrast agent molecules could freely diffuse within the cartilage. This model does not fully reflect the complicated processes that occur in an active joint. Many factors were ignored to simplify the experimental design, such as pressure from the marrow cavity, which may resist the downward penetration of the contrast agent. In addition, the relaxation of compressed cartilage was not taken into account because of the limitations of our equipment. Although apparent diffusion in one direction was demonstrated, we cannot exclude the possibility of reverse diffusion from deep cartilage or subchondral bone. Because of the existence of different stages of OA from same plateau, we did not make statistical analysis for the gender effect. Moreover, in clinical CT applications, the contrast agent attains a distribution equilibrium within approximately 2 h. To avoid μCT artifacts, our custom-made loading device had no metallic electronic components. This compromise limited the precisely controlled functions to achieve. The minimum interval time for cyclic compression was inevitably limited to 30 min. As a result, it cannot cover all aspects related to the diffusion processes, and further mechanical experiments are necessary to investigate cyclic loading in particular.

In summary, this study investigated the diffusion processes of a contrast agent within osteoarthritic cartilage using CEμCT, under different types of compression. Variations in the diffusion curves and coefficients were generally attributed to the loading patterns and histologic changes in both cartilage and subchondral bone. These data could be used to assess OA cartilage and enhance drug-injection therapies that target the OA joint cavity. For example, the extent of drug penetration depends mainly on the permeability and pathological features of degenerated cartilage. In particular, cyclic compression can significantly accelerate solute transport, except within late-stage OA cartilage, which has inadequate resilience. This suggests that restricting joint movements following drug injection could prevent an effective dose in the joint cavity from decreasing too quickly. Although further studies are needed to verify diffusion measurement using clinic instruments, the CEμCT method combined with cyclic loading could be effective for simultaneously regulating and observing the diffusion of drugs in patients with joint disease.

Funding

Declaration of competing interest

All authors declare that they have no conflict of interest.

References

[1] Mow VC, Wang CC, Hung CT. The extracellular matrix, interstitial fluid and ions as a mechanical signal transducer in articular cartilage. Osteoarthr Cartil 1999;7(1):41–58.

[2] Lories RJ, Luyten FP. The bone-cartilage unit in osteoarthritis. Nat Rev Rheumatol 2011;7(1):43–9.

[3] Funck-Brentano T, Cohen-Solal M. Crosstalk between cartilage and bone: when bone cytokines matter. Cytokine Growth Factor Rev 2011;22(2):91–7.

[4] O'Hara BP, Urban JP, Maroudas A. Influence of cyclic loading on the nutrition of articular cartilage. Ann Rheum Dis 1990;49:536–9.

[5] Felson DT. Osteoarthritis as a disease of mechanics. Osteoarthr Cartil 2013;21(1):10–5.

[6] Arkill KP, Winlove CP. Solute transport in the deep and calcified zones of articular cartilage. Osteoarthr Cartil 2008;16(6):708–14.

[7] Gardiner B, Smith D, Pivonka P, Grodzinsky A, Frank E, Zhang L. Solute transport in cartilage undergoing cyclic deformation. Comput Methods Biomech Biomed Eng 2007;10(4):265–78.

[8] Zhang L, Gardiner BS, Smith DW, Pivonka P, Grodzinsky A. The effect of cyclic deformation and solute binding on solute transport in cartilage. Arch Biochem Biophys 2007;457(1):47–56.

[9] Nimer E, Schneiderman R, Maroudas A. Diffusion and partition of solutes in cartilage under static load. Biophys Chem 2003;106(2):125–46.

[10] Shafieyan Yousef, Khosravi Niloufar, Moeini Mohammed, Quinn TM. Diffusion of MRI and CT contrast agents in articular cartilage under static compression. Biophys J 2014;107:485–92.

[11] Quinn TM, Morel V, Meister JJ. Static compression of articular cartilage can reduce solute diffusivity and partitioning: implications for the chondrocyte biological response. J Biomech 2001;34:1463–9.

[12] Wang X, Ayati BP, Brouillete MJ, Graham JM, Ramakrishnan PS, Martin JA. Modelling and simulation of the effects of cyclic loading on articular cartilage lesion formation. Int J Numer Method Biomed Eng 2014;30(10):927–41.

[13] DiDomenico CD, Xiang Wang Z, Bonassar LJ. Cyclic mechanical loading enhances transport of antibodies into articular cartilage. J Biomech Eng 2017;139(1).

[14] Korhonen M S RK, Toyras LJ, Rieppo J, Hirvonen J, Helminen HJ, Jurvelin JS. Comparison of the equilibrium response of articular cartilage in unconfined compression, confined compression and indentation. J Biomech 2002;35:903–9.

[15] vander Sluijs R G T G JA, vander Linden AJ, Bulstra SK, Kuyer R, Drukker J. The reliability of the Mankin score for osteoarthritis. J Orthop Res 1992;10(1):58–61.

[16] Stewart RC, Honkanen JTJ, Kokkonen HT, Tiitu V, Saarakkala S, Joukainen A, et al. Contrast-enhanced computed tomography enables quantitative evaluation of tissue properties at intrajoint regions in cadaveric knee cartilage. Cartil 2017;8(4):391–9.

[17] Martin Seitz A, Galbusera F, Krais C, Ignatius A, Durselen L. Stress-relaxation response of human menisci under confined compression conditions. J Mech Behav Biomed Mater 2013;26:68–80.

[18] Silvast TS, Jurvelin JS, Lammi MJ, Toyras J. pQCT study on diffusion and equilibrium distribution of iodinated anionic contrast agent in human articular cartilage–associations to matrix composition and integrity. Osteoarthr Cartil 2009;17(1):26–32.

[19] Kulmala KA, Korhonen RK, Julkunen P, Jurvelin JS, Quinn TM, Kroger H, et al. Diffusion coefficients of articular cartilage for different CT and MRI contrast agents. Med Eng Phys 2010;32(8):878–82.

[20] Aula AS, Jurvelin JS, Toyras J. Simultaneous computed tomography of articular cartilage and subchondral bone. Osteoarthr Cartil 2009;17(12):1583–8.

[21] Lakin BA, Ellis DJ, Shelofsky JS, Freedman JD, Grinstaff MW, Snyder BD. Contrast-enhanced CT facilitates rapid, non-destructive assessment of cartilage and bone properties of the human metacarpal. Osteoarthritis Cartilage 2015;23(12):2158–66.

[22] Silvast TS, Kokkonen HT, Jurvelin JS, Quinn TM, Nieminen MT, Töyräs J. Diffusion and near-equilibrium distribution of MRI and CT contrast agents in articular cartilage. PhysMed Biol 2009;54(22):6823–36.

[23] Honkanen JT, Turunen MJ, Freedman JD, Saarakkala S, Grinstaff MW, Ylarinne JH, et al. Cationic contrast agent diffusion differs between cartilage and meniscus. Ann Biomed Eng 2016;44(10):2913–21.

[24] Arbabi V, Pouran B, Weinans H, Zadpoor AA. Transport of neutral solute across articular cartilage: the role of zonal diffusivities. J Biomech Eng 2015;137(7):071001.

[25] Boschetti F, Peretti GM. Tensile and compressive properties of healthy and osteoarthritic human articular cartilage. Biorheology 2008;45(3–4):337–44.

[26] Grenier S, Bhargava MM, Torzilli PA. An in vitro model for the pathological degradation of articular cartilage in osteoarthritis. J Biomech 2014;47(3):645–52.

[27] Silvast TS, Jurvelin JS, Aula AS, Lammi MJ, Toyras J. Contrast agent-enhanced computed tomography of articular cartilage: association with tissue composition and properties. Acta Radiol 2009;50(1):78–85.

[28] Guangyi Li JY, Gao Junjie, Cheng Tak S, Pavlos Nathan J, Zhang Changqing, Zheng Ming H. Subchondral bone in osteoarthritis: insight into risk factors and microstructural changes. Arthritis Res Ther 2013;15:223–35.

[29] Hwang J, Bae WC, Shieu W, Lewis CW, Bugbee WD, Sah RL. Increased hydraulic conductance of human articular cartilage and subchondral bone plate with progression of osteoarthritis. Arthritis Rheum 2008;58(12):3831–42.